Robust Image Matching under a Large Disparity

Yasushi Kanazawa* and Kenichi Kanatani†

*Department of Knowledge-based Information Engineering
Toyohashi University of Technology, Toyohashi, Aichi 441-8580 Japan
†Department of Information Technology, Okayama University, Okayama 700-8530 Japan
kanazawa@tutkie.tut.ac.jp, kanatani@suri.it.okayama-u.ac.jp

Summary

We present a new method for detecting point matches between two images that have a large disparity resulting from camera rotations and zooming changes. Our strategy is to impose various constraints such as local image correlations, spatial consistency, and global smoothness as "soft" constraints via their "confidence" before imposing the "hard" epipolar constraint by RANSAC. We also introduce a model selection procedure to test if the image mapping can be regarded as a homography. We demonstrate the effectiveness of our method by real image examples.

1. Introduction

Establishing point correspondences over multiple images is the first step of many computer vision applications. Two approaches exist for this purpose: tracking correspondences over successive frames, and direct matching between separate frames. This paper focuses on the latter.

The basic principle is local correlation measurement by template matching. Detecting feature points in the first and second images separately using a corner detector [3, 12], we measure the correlation between the neighborhoods of the two points for each candidate pair and match those that have a high correlation. This works very well if one image is a translated copy of the other. However, if the two images are taken from different positions in the scene, the corresponding parts in the images appear differently with local deformations that depend on the 3-D shape of that part of the scene and its orientation relative to the two camera positions. The template correlation is very much affected by such local deformations. In particular, the correlation significantly diminishes if the camera is rotated or zooming takes place during the image capturing process.

It follows that local correlations alone are not sufficient for establishing correspondences. We need some constraints on the two images. If the scene is a planar surface or in the distance, the two images are related by an image transformation called *homography* [4]. This strong constraint can be combined with voting techniques such as LMedS [11] and RANSAC [2] to match the images robustly. Analyzing the template residual [7], the authors have proposed a hierarchical voting scheme called *stratified matching* for robustly matching two images even in the presence of a large image deformations [10].

For a general scene, on the other hand, the only available constraint is what is known as the *epipolar equation* [4], and various types of voting schemes based on it have been proposed [1, 4, 15]. However, the epipolar equation is a very weak constraint. In fact, a lot of wrong matches, which humans could easily detect, satisfy this constraint. As a result, the combination of local image correlations and the epipolar equation works only when the disparity is relatively small with small camera rotations and small zooming changes.

In this paper, we pursue a robust matching technique that works even in the presence of a large disparity involving camera rotations and zooming changes. For this, local correlations and the epipolar constraint are not sufficient; we need additional constraints.

First, we require that correct matches to be fairly smooth and consistent, assuming that the scene does not have an extraordinary 3-D shape. We also assume that the scene is more or less planar or in the distance so that the image transformation can be roughly approximated by a homography.

However, *none of these constraints should be imposed definitively*. Even if two points have low image correlations, we cannot deny the possibility that they may match. Similarly, non-smooth or seemingly inconsistent matches can be correct. Let us say such violable constraints are *soft* while inviolable constraints such as the epipolar equation are *hard*.

In order to impose soft constraints, we introduce *confidence values* to *all* potential matches in such a way that those that satisfy the constraints well have high confidence, yet none of them is definitively rejected. On the other hand, the hard epipolar constraint is strictly imposed by RANSAC. In other words, we favor, among those matches that strictly satisfy the

epipolar equation, those that have high confidence of the soft constraints.

We first describe the soft constraints that we require and the assignment of their confidence. Then, we describe the voting procedure that combines the soft constraints and the hard epipolar equation. We also describe a model selection procedure to test if the image mapping can be regarded as a homography. Finally, we show real image examples to demonstrate that our method is very effective even when conventional methods fail.

2. Template Matching

We measure the local correlations between the neighborhoods of point p in the first image and point q in the second by the *residual (sum of squares)*

$$J(p,q) = \sum_{(i,j)\in\mathcal{N}} |T_p(i,j) - T_q(i,j)|^2, \qquad (1)$$

where $T_p(i,j)$ and $T_q(i,j)$ are the intensity values of the templates defined by cutting out an $w \times w$ pixel region $\mathcal{N}$ centered on p and q, respectively[1].

The basic procedure for point matching is as follows. We extract N points $p_1, ..., p_N$ in the first image and M points $q_1, ..., q_M$ in the second, using a feature detector such as the Harris operator [3] and SUSAN [12]. Then, we compute the residuals $\{J(p_\alpha, q_\beta)\}$, $\alpha = 1, ..., N$, $\beta = 1, ..., M$, for all NM combinations of the extracted points. We search the $N \times M$ table of $\{J(p_\alpha, q_\beta)\}$ for the minimum value $J(p_{\alpha*}, q_{\beta*})$ and establish the match between points $p_{\alpha*}$ and $q_{\beta*}$. Then, we remove from the table the column and row that contain the value $J(p_{\alpha*}, q_{\beta*})$ and do the same procedure to the resulting $(N-1) \times (N-1)$ table. Repeating this, we end up with $L = \min(N, M)$ matches. We call this procedure *uniqueness enforcement* with respect to the residual J.

However, this procedure cannot be done directly, since the selected pairs may not be all correct while some of the discarded pairs may be correct. In order to take all potential matches into consideration, we introduce confidence values to all pairs.

3. Confidence of Local Correlations

We define the *confidence* of local correlations for the pair (p, q) via the *Gibbs distribution* in the form

$$P = e^{-sJ(p,q)}, \qquad (2)$$

so that a high confidence is given for a smaller residual $J(p, q)$. Physicists usually put $s = 1/kT$ and call T *temperature*, where k is the Boltzmann constant. If

$s = 0$ (or $T = \infty$), we uniformly have $P = 1$ irrespective of the residual $J(p, q)$. As s increases (or T decreases), the confidence of those with large residuals quickly decreases, and ultimately the confidence concentrates only on the smallest residual.

Here, we determine the value of s as follows. Among all the NM pairs $\{(p_\alpha, q_\beta)\}$, at most $L (= \min(N, M))$ of them can be correct. We require that the average of the L smallest residuals equal the overall weighted average with respect to the confidence (2). If the NM potential matches (p_α, q_β) are sorted according to their residuals $J(p_\alpha, q_\beta)$ in ascending order and the λth residual is abbreviated as J_λ, this condition is written in the form

$$\frac{1}{Z}\sum_{\lambda=1}^{NM} J_\lambda e^{-sJ_\lambda} = \bar{J}, \qquad (3)$$

where

$$Z = \sum_{\lambda=1}^{NM} e^{-sJ_\lambda}, \qquad \bar{J} = \frac{1}{L}\sum_{\lambda=1}^{L} J_\lambda. \qquad (4)$$

The solution of eq. (3) is easily computed by Newton iterations to search for the zero of $\Phi(s) = 0$, starting from $s = 0$, where we define

$$\Phi(s) = \sum_{\lambda=1}^{NM} (J_\lambda - \bar{J}) e^{-sJ_\lambda}. \qquad (5)$$

Let $P_\lambda^{(0)}$ be the thus defined confidence of local correlations for the λth pair.

4. Confidence of Spatial Consistency

Next, we introduce the confidence of spatial consistency, assuming that the scene does not have an extraordinary 3-D shape so that correct matches are fairly consistent.

For this, we choose tentative candidates for correct matches by enforcing uniqueness with respect to $P_\lambda^{(0)}$ to those pairs that satisfy[2]

$$P_\lambda^{(0)} > e^{-k^2/2}. \qquad (6)$$

We enumerate the resulting matches by the index $\mu = 1, ..., n_0$ in an arbitrary order. Let $\vec{r}_\mu$ be the 2-dimensional vector that connects the two points of the μth match, starting from the one in the first image and ending at the other in the second. We call it the "flow vector" of the μth match.

Our strategy is to view those matches which are consistent with the resulting "optical flow" $\{\vec{r}_\mu\}$ as more likely to be correct. Specifically, we compute the confidence weighted mean $\vec{r}_m$ and the confidence weighted

---

[1]We let $w = 9$ in our experiments.

[2]we let $k = 3$ in our experiment.

covariance matrix V of the optical flow by

$$\vec{r}_m = \frac{1}{Z} \sum_{\mu=1}^{n_0} P_\mu^{(0)} \vec{r}_\mu, \quad Z = \sum_{\mu=1}^{n_0} P_\mu^{(0)},$$

$$V = \frac{1}{Z} \sum_{\lambda=1}^{n_0} P_\mu^{(0)} (\vec{r}_\mu - \vec{r}_m)(\vec{r}_\mu - \vec{r}_m)^\top. \quad (7)$$

Now, we go back to the original NM potential matches. We define their confidence of spatial consistency via the Gaussian distribution in the form

$$P_\lambda^{(1)} = e^{-(\vec{r}_\lambda - \vec{r}_m, V^{-1}(\vec{r}_\lambda - \vec{r}_m))}, \quad (8)$$

where $(\vec{a}, \vec{b})$ designates the inner product of vectors $\vec{a}$ and $\vec{b}$. Thus, a flow vector $\vec{r}_\lambda$ has a low confidence if it largely deviates from the optical flow $\{\vec{r}_\mu\}$.

5. Confidence of Global Smoothness

We then introduce the confidence of global smoothness, assuming that the scene is more or less planar or in the distance so that the image transformation can be roughly approximated by a homography.

As in the case of spatial consistency, we first choose tentative candidates for correct matches. This time, we enforce uniqueness with respect to $P_\lambda^{(0)} P_\lambda^{(1)}$ to those pairs that satisfy

$$P_\lambda^{(0)} P_\lambda^{(1)} > e^{-2k^2/2}. \quad (9)$$

We enumerate the resulting matches by the index $\mu = 1, ..., n_1$ in an arbitrary order.

Let (x_μ, y_μ) and (x'_μ, y'_μ) be the two points of the μth pair. We represent these two points by 3-D vectors

$$\boldsymbol{x}_\mu = \begin{pmatrix} x_\mu/f_0 \\ y_\mu/f_0 \\ 1 \end{pmatrix}, \quad \boldsymbol{x}'_\mu = \begin{pmatrix} x'_\mu/f_0 \\ y'_\mu/f_0 \\ 1 \end{pmatrix}, \quad (10)$$

where f_0 is an appropriate scale factor, e.g., the image size. In this vector representation, a *homography* is written as an image mapping in the form

$$\boldsymbol{x}' = Z[\boldsymbol{H}\boldsymbol{x}], \quad (11)$$

where $Z[\cdot]$ means normalization to make the third component 1.

We optimally fit a homography to the n_1 candidate matches. Let the true values (in the absence of noise) of $\{\boldsymbol{x}_\mu\}$ and $\{\boldsymbol{x}'_\mu\}$ be, respectively, $\{\bar{\boldsymbol{x}}_\mu\}$ and $\{\bar{\boldsymbol{x}}'_\mu\}$ (their third components are identically 1). Taking account of their confidence, we compute the homography matrix $\boldsymbol{H}$ by minimizing

$$J = \sum_{\mu=1}^{n_1} P_\mu^{(0)} P_\mu^{(1)} (\|\boldsymbol{x}_\mu - \bar{\boldsymbol{x}}_\mu\|^2 + \|\boldsymbol{x}'_\mu - \bar{\boldsymbol{x}}'_\mu\|^2), \quad (12)$$

subject to the constraint $\bar{\boldsymbol{x}}'_\mu = Z[\boldsymbol{H}\bar{\boldsymbol{x}}_\mu]$, $\mu = 1, ..., n_1$, with respect to $\{\bar{\boldsymbol{x}}_\mu\}$, $\{\bar{\boldsymbol{x}}'_\mu\}$, and $\boldsymbol{H}$. The solution is easily obtained by modifying the optimization technique called *renormalization*[3] [8]

Now, we go back to the original NM potential matches. The discrepancy of each potential match from the estimated homography is measured by

$$D_\lambda^H = \|\boldsymbol{x}'_\lambda - Z[\boldsymbol{H}\boldsymbol{x}_\lambda]\|^2, \quad (13)$$

where $\boldsymbol{x}_\lambda$ and $\boldsymbol{x}'_\lambda$ represent the two points of the λth pair, $\lambda = 1, ..., NM$. We define the confidence of global smoothness via the Gibbs distribution in the same way as the confidence of local correlations. Namely, we let

$$P_\lambda^{(2)} = e^{-tD_\lambda^H}. \quad (14)$$

The constant t is determined by solving

$$\frac{1}{Z} \sum_{\lambda=1}^{NM} D_\lambda^H e^{-tD_\lambda^H} = \bar{D}^H, \quad (15)$$

where

$$Z = \sum_{\lambda=1}^{NM} e^{-tD_\lambda^H}, \quad \bar{D}^H = \frac{1}{L} \sum_{\lambda=1}^{L} D_\lambda^H. \quad (16)$$

The solution is easily obtained by doing Newton iterations to eq. (5) after J_λ is replaced by D_λ^H.

6. Voting the Epipolar Constraint

Finally, we strictly enforce the *epipolar constraint*. In vector representation, we have for a matching pair $\{\boldsymbol{x}, \boldsymbol{x}'\}$ the following *epipolar equation* [4]:

$$(\boldsymbol{x}, \boldsymbol{F}\boldsymbol{x}') = 0. \quad (17)$$

Here, $\boldsymbol{F}$ is a singular matrix with rank 2, called the *fundamental matrix* [4]. It is defined only up to an arbitrary scale factor.

First, we choose tentative candidates for correct matches by enforcing uniqueness with respect to $P_\lambda^{(0)} P_\lambda^{(1)} P_\lambda^{(2)}$ to those pairs that satisfy

$$P_\lambda^{(0)} P_\lambda^{(1)} P_\lambda^{(2)} > e^{-3k^2/2}. \quad (18)$$

We enumerate the resulting matches by the index $\mu = 1, ..., n_2$ in an arbitrary order. From these candidate matches, we robustly fit the epipolar equation (17) using RANSAC [2, 4]. Letting $S_m = 0$ and $\boldsymbol{F}_m = \boldsymbol{O}$ as initial values, we do the following computation:

1. Randomly choose eight among the n_2 pairs.

---

[3] The C++ program is publicly available at
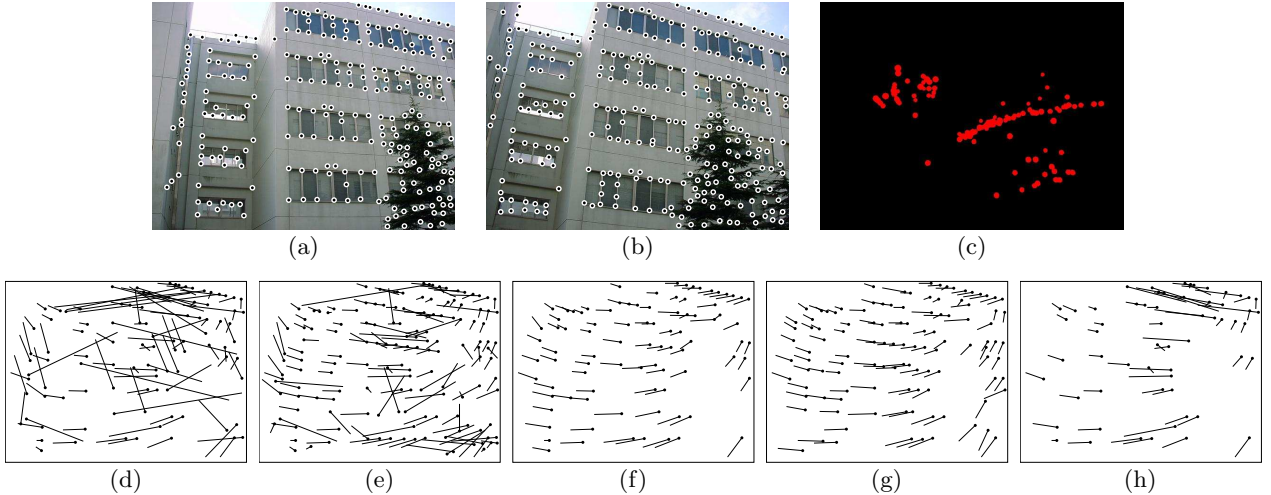http://www.suri.it.okayama-u.ac.jp/

Figure 1: (a), (b) Input images and detected feature points. (c) 3-D reconstruction computed from the final matches (top view). (d) Initial matches based on local correlations. (e) Matches with spatial consistency incorporated. (f) Matches with global smoothness added. (g) Final matches with the epipolar constraint imposed. (h) Matches obtained from (d) by direct RANSAC.

2. From them, compute the fundamental matrix $\boldsymbol{F}$. Since the scale of $\boldsymbol{F}$ is indeterminate, the nine elements of $\boldsymbol{F}$ are easily obtained from the eight pairs by solving linear equations.

3. For each of the n_2 pairs, compute

$$D_\mu^F = \frac{(\boldsymbol{x}_\mu, \boldsymbol{F}\boldsymbol{x}'_\mu)^2}{\|\boldsymbol{P_k}\boldsymbol{F}^\top \boldsymbol{x}_\mu\|^2 + \|\boldsymbol{P_k}\boldsymbol{F}\boldsymbol{x}'_\mu\|^2}, \qquad (19)$$

where $\boldsymbol{P_k} = \mathrm{diag}(1, 1, 0)$ (the diagonal matrix with diagonal elements 1, 1, and 0 in that order).

4. Let S the sum of the confidence $P_\mu^{(0)}P_\mu^{(1)}P_\mu^{(2)}$ of those pairs that satisfy

$$D_\mu^F \leq \frac{2d^2}{f_0^2}, \qquad (20)$$

where d (pixel) is a user definable threshold[4].

5. If $S > S_m$, update $S_m \leftarrow S$ and $\boldsymbol{F}_m \leftarrow \boldsymbol{F}$.

We repeat this computation a sufficient number of times to find the matrix $\boldsymbol{F}_m$ that gives the largest total confidence S_m.

Now, we go back to the original NM potential matches. The degree of fit to the epipolar equation is measured by D_λ^F in eq. (19) if $\boldsymbol{x}_\mu$ and $\boldsymbol{x}'_\mu$ are replaced, respectively, by $\boldsymbol{x}_\lambda$ and $\boldsymbol{x}'_\lambda$ that represent the λth pair, $\lambda = 1, ..., NM$. We choose from among the NM pairs those that satisfy eq. (20). The resulting pairs are thresholded by the criterion (18). Finally, we enforce uniqueness with respect to $P_\lambda^{(0)}P_\lambda^{(1)}P_\lambda^{(2)}$ to obtain the final matches.

---
[4]We let $d = 3$ in our experiment.

7. Model Selection

If the scene is a planar surface or in the distance, the image mapping between the two images is a homography, which allows us to determine the image mapping pixelwise. This information can be used to generate a panoramic image [10], whereas we cannot reconstruct the 3-D structure of the scene without additional information. So, it is crucial to see if the image mapping is a homography.

A naive idea is to fit the homography relation and the epipolar constraint to the obtained matches and decide that the mapping is a homography if the residual for the homography is smaller than for the epipolar constraint. This does not work, however, because the homography is a stronger constraint than the epipolar equation, which is always satisfied. As a result, the residual for the homography is never smaller than for the epipolar constraint.

Thus, we need to balance the strength of the constraint with the increase in the residual. This can be done by *model selection* using, among other measures, the *geometric AIC* [6] (see [13, 14] for other criteria). Let n be the number of the finally obtained matches. We fit the homography relation and the epipolar constraint to the n matches in an optimal manner and compute their respective residuals J^H and J^F (see [5] for the details of the computation). Their geometric AICs are respectively given by

$$\begin{aligned} \text{G-AIC}^H &= J^H + 2(2n + 8)\epsilon^2, \\ \text{G-AIC}^F &= J^F + 2(3n + 7)\epsilon^2, \end{aligned} \qquad (21)$$

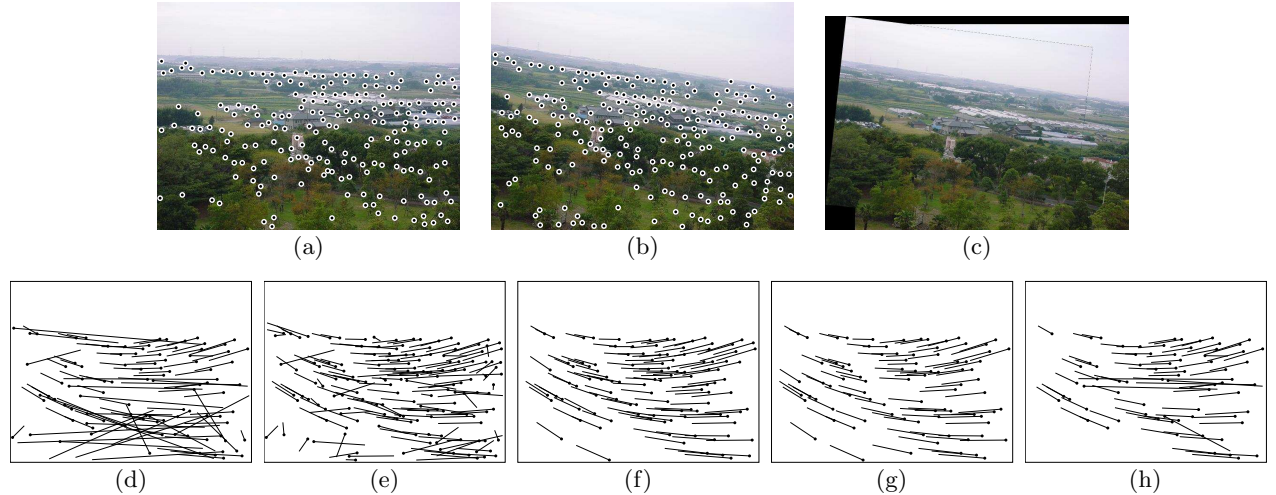where ϵ is a constant that specifies the degree of image

Figure 2: (a), (b) Input images and detected feature points. (c) Panoramic image generated from the final matches. (d) Initial matches based on local correlations. (e) Matches with spatial consistency incorporated. (f) Matches with global smoothness added. (g) Final matches with the epipolar constraint imposed. (h) Matches obtained from (d) by direct RANSAC.

noise. It is estimated from the residual of the general epipolar constraint as follows [5]:

$$\hat{\epsilon}^2 = \frac{J^F}{n-7}. \tag{22}$$

The image relationship is regarded as a homography if G-AIC^H < G-AIC^F.

8. Real Image Examples

Figs. 1(a) and (b) show two images of an outdoor scene. We detected 300 feature points from each image using the Harris operator [3], as marked there. Fig. 1(d) shows the "optical flow" of the initial candidate matches based on local correlations. As we can see, this scene has many periodic patterns, so the template matching based only on local correlations produce many mismatches.

Fig. 1(e) is the matches after spatial consistency is imposed, and Fig. 1(f) is the matchers after global smoothness is added. We see that the accuracy increases as we impose more constraints. Doing RANSAC to the matches in Fig. 1(f), we obtained the final matches in Fig. 1(g).

For comparison, the optical flow obtained by directly doing RANSAC to the initial matches in Fig. 1(d) is shown in Fig. 1(h). As we can see, many wrong matches are included.

Thus, our procedure is very effective in narrowing down the correct matches by gradually incorporating various soft constraints through their confidence. As a result, we can obtain correct matches accurately and robustly even when the disparity is large.

Comparing the geometric AICs computed from the final matches, we can conclude that in this case the image mapping cannot be regarded as a homography. Fig. 1(c) shows the 3-D shape reconstructed from the computed fundamental matrix $\boldsymbol{F}$ (top view). We used the method described in [9].

Fig. 2 shows another example similarly arranged. There is a slight camera rotation between Figs. 2(a) and (b), and the scene has many similar textures, so considerable mismatches occurred by template matching based on local correlations alone. However, our method successfully generated many correct matches as compared with direct RANSAC. This time, the image transformation can be regarded as a homography. Fig. 2(c) shows the panoramic image generated by the computed homography.

We also examined the effects of camera rotations and zooming changes using the images in Figs. 3 and 4. These images consist in large part of almost identical periodic patterns with very similar textures, so matching by local correlation alone is extremely difficult. Yet, our method successfully generated sufficiently many correct matches.

Figs. 3(a) and (b) are the original image pair, and Figs. 3(c) and (d) are obtained by rotating the image in Figs. 3(b) by 5 and 10 degrees, respectively. The matches in the top row are obtained from the pair (a) and (b); the matches in the middle row are obtained from the pair (a) and (c); the matches in the bottom row are obtained from the pair (a) and (d). In each row, (e)∼(i) are the result corresponding to (d)∼(h) in Figs. 1 and 2.
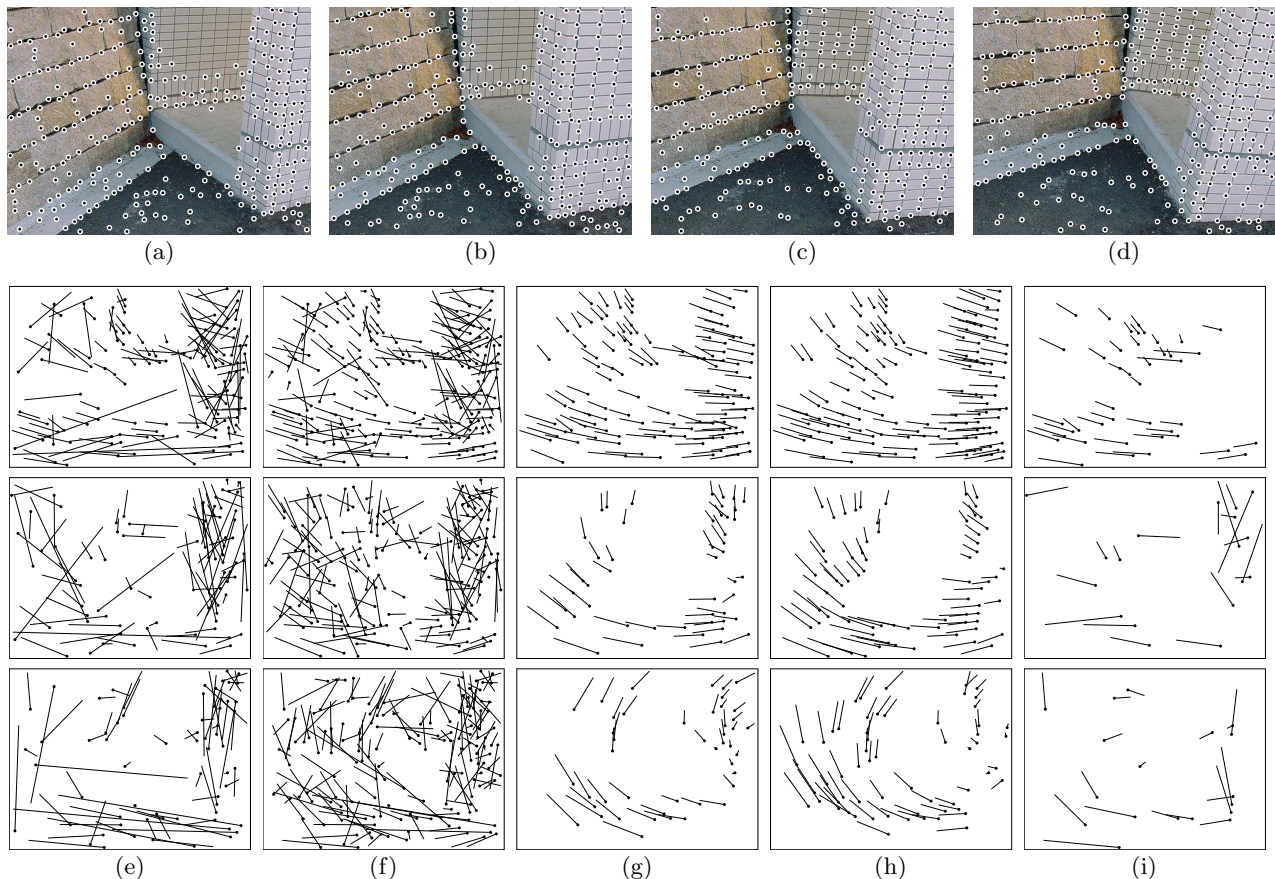
Figs. 4(a) and (b) are another image pair, and

Figure 3: Effects of image rotations: (a) Left image. (b) Right image. (c) Rotation of (b) by 5°. (d) Rotation of (b) by 10°. The results from the pair (a) and (b) (top row), the pair (a) and (c) (middle row), and the pair (a) and (d) (bottom row): (e) Initial matches based on local correlations. (f) Matches with spatial consistency incorporated. (g) Matches with global smoothness added. (h) Final matches with the epipolar constraint imposed. (i) Matches obtained from (e) by direct RANSAC.

Figs. 4(c) and (d) are obtained by zooming out the image in Figs. 4(b) by 80% and 65%, respectively. The rest is arranged in the same way as in Figs. 3.

From these, we can see that our method is robust to image rotations and zooming changes. For the above examples, the total computation time of our method (including loading image files, feature point extraction, and outputting debug information) was 23 sec on average, while direct RANSAC took 14 sec on average. We used Pentium III 700MHz for the CPU with 768MB main memory and Linux for the OS. Thus, we can gain accuracy and robustness at a relatively small computational cost.

9. Conclusions

We have presented a new method for detecting point matches between two images that have a large disparity involving camera rotations and zooming changes. Our strategy is to impose various constraints such as local image correlations, spatial consistency, and global smoothness as "soft" constraints in the form of their "confidence" before imposing the "hard" epipolar constraint by RANSAC. We have also introduced a model selection procedure to test if the image mapping can be regarded as a homography. We have demonstrated the effectiveness of our method by real image examples.

References

[1] P. Beardsley, P. Torr and A. Zisserman, 3D model acquisition from extended image sequences, *Proc. 4th Euro. Conf. Comput. Vision*, April 1996, Cambridge, U.K., Vol. 2, pp. 683–695.

[2] M. A. Fischler and R. C. Bolles, Random sample consensus: A paradigm for model fitting with applications
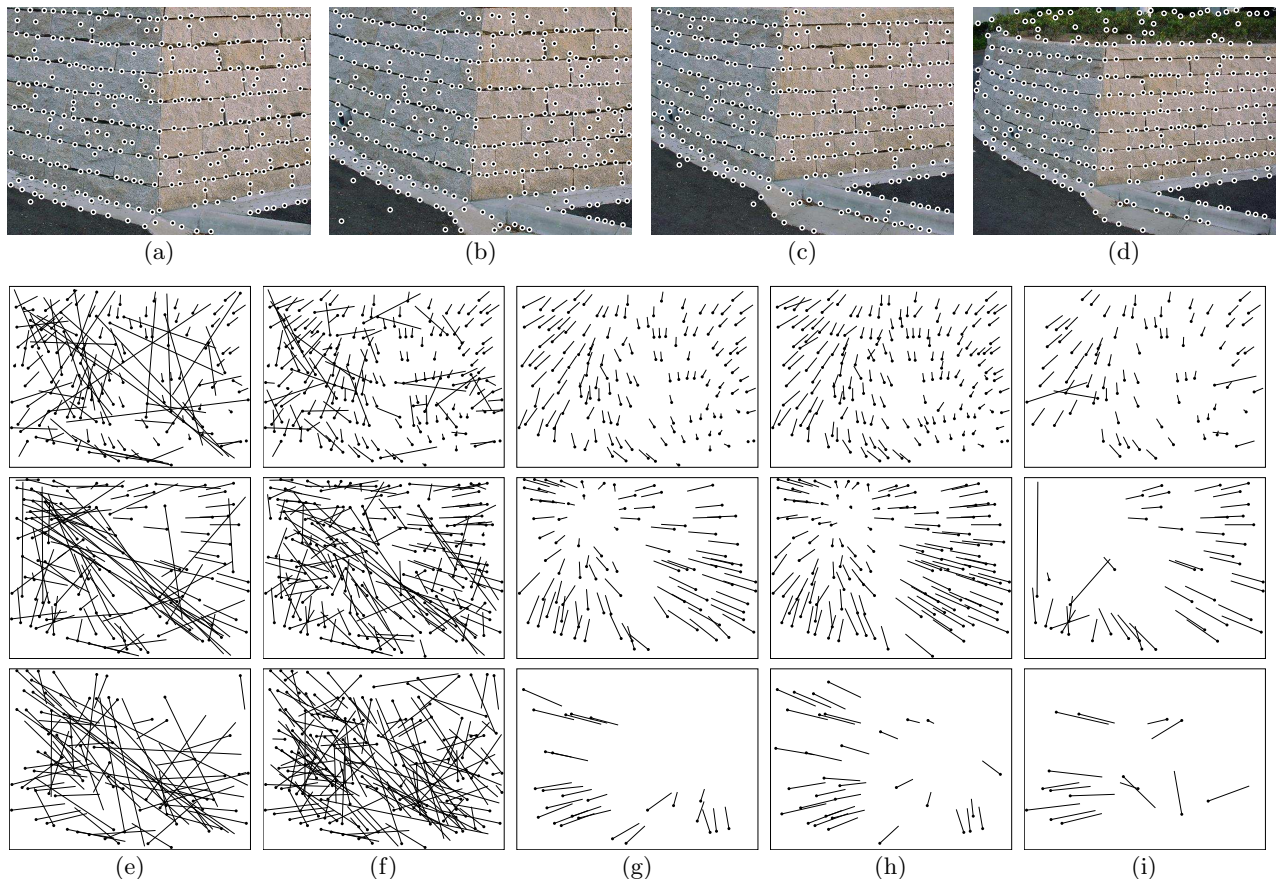
Figure 4: Effects of zooming changes: (a) Left image. (b) Right image. (c) Zooming out of (b) by 80%. (d) Zooming out of (b) by 65%. The results from the pair (a) and (b) (top row), the pair (a) and (c) (middle row), and the pair (a) and (d) (bottom row): (e) Initial matches based on local correlations. (f) Matches with spatial consistency incorporated. (g) Matches with global smoothness added. (h) Final matches with the epipolar constraint imposed. (i) Matches obtained from (e) by direct RANSAC.

to image analysis and automated cartography, *Comm. ACM*, **24**-6 (1981), 381–395.

[3] C. Harris and M. Stephens, A combined corner and edge detector, *Proc. 4th Alvey Vision Conf.*, August 1988, Manchester, U.K., pp. 147–151.

[4] R. Hartley and A. Zisserman, *Multiple View Geometry in Computer Vision*, Cambridge University Press, Cambridge, U.K., 2000.

[5] K. Kanatani, *Statistical Optimization for Geometric Computation: Theory and Practice*, Elsevier Science, Amsterdam, the Netherlands, 1996.

[6] K. Kanatani, Geometric information criterion for model selection, *Int. J. Comput. Vision*, **26**-3 (1998), 171–189.

[7] K. Kanatani and Y. Kanazawa, Automatic thresholding for correspondence detection, *Proc. Workshop on Statistical Methods in Video Processing*, June 2002, Denmark, Copenhagen, pp. 19–24.

[8] K. Kanatani and N. Ohta, Accuracy bounds and optimal computation of homography for image mosaicing applications, *Proc. 7th Int. Conf. Comput. Vision*, September 1999, Kerkyra, Greece, Vol. 1, pp. 73–78.

[9] K. Kanatani and N. Ohta, Comparing optimal 3-D reconstruction for finite motion and optical flow, *Mem-oirs of the Faculty of Engineering, Okayama University*, **36**-1 (2001), 91–106.

[10] Y. Kanazawa and K. Kanatani, Image mosaicing by stratified matching, *Workshop on Statistical Methods in Video Processing*, June 2002, Denmark, Copenhagen, pp. 31–36.

[11] P. J. Rousseeuw and A. M. Leroy, *Robust Regression and Outlier Detection*, Wiley, New York, 1987.

[12] S. M. Smith and J. M. Brady, SUSAN—A new approach to low level image processing, *Int. J. Comput. Vision*, **23**-1 (1997), 45–78.

[13] P. H. S. Torr, An assignment of information criteria for motion model selection, *Proc. IEEE Conf. Comput. Vision Patt. Recog.*, Puerto Rico, June 1997, pp. 47–53.

[14] P. H. Torr and A. Zisserman, Robust detection of degenerate configurations while estimating the fundamental matrix, *Comput. Vision Image Understand.*, **71**-3 (1998), 312–333.

[15] Z. Zhang, R. Deriche, O. Faugeras and Q.-T. Luong, A robust technique for matching two uncalibrated images through the recovery of the unknown epipolar geometry, *Artif. Intell.*, **78** (1995), 87–119.